Atmos. Chem. Phys. Discuss., 15, 481–519, 2015
www.atmos-chem-phys-discuss.net/15/481/2015/
doi:10.5194/acpd-15-481-2015

Atmospheric Chemistry and Physics Discussions

Drivers of the tropospheric ozone budget throughout the 21st century under the medium-high climate scenario RCP 6.0

L. E. Revell[1], F. Tummon[1], A. Stenke[1], T. Sukhodolov[1,2], A. Coulon[1], E. Rozanov[1,2], H. Garny[3], V. Grewe[3], and T. Peter[1]

[1]Institute for Atmospheric and Climate Science, ETH Zurich, Zurich, Switzerland
[2]Physical-Meteorological Observatory/World Radiation Center, Davos, Switzerland
[3]DLR, Institut für Physik der Atmosphäre, Oberpfaffenhofen, Germany

Received: 18 September 2014 – Accepted: 11 November 2014 – Published: 7 January 2015

Correspondence to: L. E. Revell (laura.revell@env.ethz.ch)

Published by Copernicus Publications on behalf of the European Geosciences Union.

Abstract

Because tropospheric ozone is both a greenhouse gas and harmful air pollutant, it is important to understand how anthropogenic activities may influence its abundance and distribution through the 21st century. Here, we present model simulations performed with the chemistry-climate model SOCOL, in which spatially disaggregated chemistry and transport tracers have been implemented in order to better understand the distribution and projected changes in tropospheric ozone. We examine the influences of ozone precursor emissions (nitrogen oxides (NO_x), carbon monoxide (CO) and volatile organic compounds (VOCs)), climate change and stratospheric ozone recovery on the tropospheric ozone budget, in a simulation following the climate scenario Representative Concentration Pathway (RCP) 6.0. Changes in ozone precursor emissions have the largest effect, leading to a global-mean increase in tropospheric ozone which maximises in the early 21st century at 23 %. The increase is most pronounced at northern midlatitudes, due to regional emission patterns: between 1990 and 2060, northern midlatitude tropospheric ozone remains at constantly large abundances: 31 % larger than in 1960. Over this 70 year period, attempts to reduce emissions in Europe and North America do not have an effect on zonally-averaged northern midlatitude ozone because of increasing emissions from Asia, together with the longevity of ozone in the troposphere. A simulation with fixed anthropogenic ozone precursor emissions of NO_x, CO and non-methane VOCs at 1960 conditions shows a 6 % increase in global-mean tropospheric ozone, and an 11 % increase at northern midlatitudes. This increase maximises in the 2080s, and is mostly caused by methane, which maximises in the 2080s following RCP 6.0, and plays an important role in controlling ozone directly, and indirectly through its influence on other VOCs and CO. Enhanced flux of ozone from the stratosphere to the troposphere as well as climate change-induced enhancements in lightning NO_x emissions also increase the tropospheric ozone burden, although their impacts are relatively small. Overall, the results show that ozone in the future is governed largely by changes in methane and NO_x; methane induces an increase in tropo-

ACPD
15, 481–519, 2015

spheric ozone that is approximately one-third of that caused by NO_x. Climate impacts on ozone through changes in tropospheric temperature, humidity and lightning NO_x remain secondary compared with emission strategies relating to anthropogenic emissions of NO_x, such as fossil fuel burning. Therefore, emission policies globally have a critical role to play in determining tropospheric ozone evolution through the 21st century.

1 Introduction

Ozone is a key trace gas in the atmosphere, with approximately 90 % residing in the stratosphere and 10 % in the troposphere. While stratospheric ozone is essential for shielding life on Earth from harmful ultraviolet (UV-B) radiation, tropospheric ozone has harmful effects because it is an air pollutant, with adverse effects on crop yields (and therefore food security), visibility (affecting all forms of traffic) and human health (West et al., 2007). Indeed, a recent study by Silva et al. (2013) found that anthropogenic ozone contributes towards 470 000 respiratory deaths globally each year. Simultaneously, tropospheric ozone is a greenhouse gas that has contributed significantly to climate change; it has the third-highest pre-industrial to present day radiative forcing after carbon dioxide (CO_2) and methane (CH_4) (Forster et al., 2007; Stevenson et al., 2013). In addition to its roles in air pollution and climate change, tropospheric ozone is important in determining the oxidation capacity of the troposphere; the hydroxyl (OH) radical is principally produced from ozone, and controls the lifetime of many atmospheric species such as CH_4 and NMVOCs (non-methane volatile organic compounds), including some halocarbons (Thompson, 1992).

Ozone exists in the troposphere as a result of in situ chemical production and transport from the stratosphere. Approximately 90 % is produced via chemical reactions between nitrogen oxides ($NO_x = NO + NO_2$), hydrocarbons and carbon monoxide (CO) during daylight hours (Denman et al., 2007); therefore air pollution policy can be expected to play a significant role in the evolution of tropospheric ozone through the

ACPD
15, 481–519, 2015

21st century and beyond. Depending on the sensitivity of ozone budget reactions to humidity and temperature, the distribution and abundance of tropospheric ozone may also be affected by climate change through the 21st century. Ozone can also be transported, either from the stratosphere (stratosphere–troposphere exchange, abbreviated to STE), or within the troposphere on long-range scales. Transport of ozone from the stratosphere is expected to increase through the 21st century as: (1) stratospheric ozone abundances will increase, due to the phase-out of ozone-depleting halogenated substances under the Montreal Protocol, and due to stratospheric cooling slowing the ozone destruction cycles (Bekki et al., 2011); (2) stratosphere-to-troposphere transport of air will accelerate due to a strengthening of the Brewer–Dobson circulation as projected by climate models, resulting from enhanced tropospheric warming and convection, and subsequent wave activity (Butchart et al., 2010). Both effects will lead to enhanced down-welling of ozone at mid- and polar latitudes. Stratospheric ozone recovery may further affect the evolution of tropospheric ozone through decreased solar actinic flux to the troposphere (Zhang et al., 2014).

In recent years as computational cost has declined, models which couple chemistry and climate (chemistry-climate models, or CCMs) have become increasingly complex, with many now including detailed tropospheric chemistry and other tropospheric processes. Morgenstern et al. (2013) used the UM-UKCA CCM to look at how climate change, stratospheric ozone recovery and methane affect ozone, although they did not consider future changes in non-methane ozone precursors. They found that climate change and stratospheric ozone recovery have approximately equal and opposite effects on surface ozone by 2050, resulting in an increase in tropospheric ozone driven by methane. Doherty et al. (2013) also investigated climate change-related effects on tropospheric ozone with an ensemble of three CCMs, and found that increased temperature and water vapour influenced surface ozone more strongly than climate change-induced enhancements in STE. Furthermore, several studies examining tropospheric ozone budgets and projections from the ACCMIP (Atmospheric Chemistry and Climate Model Intercomparison Project) ensemble of models have been published

ACPD
15, 481–519, 2015

recently (e.g. Bowman et al. (2013); Stevenson et al., (2013); Young et al. (2013)). The ensemble mean of results obtained from ACCMIP provides a useful point of reference for the results obtained in this study, and as such we refer to ACCMIP results later on.

To gain a clear insight into projected tropospheric ozone changes through the 21st century, we have implemented a suite of chemistry and transport tracers into the SOCOL (Solar Climate Ozone Links) CCM, and used them to disentangle the various factors influencing the ozone budget in the free troposphere. Here we compare projected ozone changes in a future reference simulation, which assumes emissions of NO_x, CO, CH_4 and NMVOCs according to Representative Concentration Pathway (RCP) 6.0, with those in simulations with ozone precursor emissions fixed at 1960 levels. Climate change and stratospheric ozone recovery are fully simulated in both scenarios, and the chemistry and transport tracers allow us to analyse their effects, for example by quantifying STE fluxes and tracking reaction rates for key ozone budget reactions.

2 Computational methods

2.1 The SOCOL chemistry-climate model

In order to understand the influences of ozone precursor emissions and climate change on the free tropospheric ozone budget (we focus mostly on the 500 hPa level), simulations were performed with the SOCOL v.3 CCM. Its forerunner, SOCOL v.2, was extensively evaluated in the SPARC CCMVal-2 activity (SPARC CCMVal, 2010) in two variants; SOCOL operated by the ETH-Zurich group and NIWA-SOCOL operated by NIWA (National Institute of Water and Atmospheric Research, New Zealand). Both compared reasonably with other CCMs, obtaining grades in the midrange. Since then SOCOL has undergone some significant improvements from version 2 to 3 (notably, the core general circulation model has been updated, and the transport of chemical trace species is calculated with the advection scheme of Lin and Rood (1996), rather than the hybrid scheme of Zubov et al. (1999), which was used in SOCOL v. 2); these

ACPD
15, 481–519, 2015

changes, along with their effect on model performance, have been documented in detail by Stenke et al. (2013).

SOCOL v.3 consists of the MEZON chemistry transport model (Egorova et al., 2003) and MA-ECHAM5, the middle atmosphere version of the ECHAM general circulation model (Roeckner et al., 2003), with 39 vertical levels between Earth's surface and 0.01 hPa (~ 80 km). For the present study, SOCOL was run with T42 horizontal resolution, which corresponds approximately to 2.8° × 2.8°. Dynamical processes in SOCOL are calculated every 15 min within the model, while radiative and chemical calculations are performed every two hours.

Chemical constituents are advected by a flux-form semi-Lagrangian scheme (Lin and Rood, 1996), and the chemical solver algorithm uses a Newton–Raphson iterative method taking into account 41 chemical species, 140 gas-phase reactions, 46 photolysis reactions, and 16 heterogeneous reactions. Isoprene (C_5H_8) oxidation is accounted for with the inclusion of the Mainz Isoprene Mechanism (MIM-1), which comprises 16 organic species (degradation products of isoprene) and a further 44 chemical reactions (Poeschl et al., 2000). Aside from isoprene and formaldehyde, we consider only the contribution to CO from other NMVOCs; that is, a certain fraction of the NMVOC emission is directly added to CO. For anthropogenic NMVOC emissions, the conversion factor to CO is 1.0, for biomass burning it is 0.31, and for biogenic NMVOC emissions it is 0.83. Biogenic emissions are not interactive, but follow a climatology (described in Sect. 2.2).

Photolysis rates are calculated at every chemical time step using a look-up-table approach (Rozanov et al., 1999), including effects of the solar irradiance variability. The look-up tables provide photolysis rates as a function of O_2 and O_3 columns, meaning that the photolysis scheme sees interactive ozone. The impact of clouds on photolysis rates is accounted for by including a cloud modification factor, following Chang et al. (1987). Interactive lightning NO_x is calculated via a parameterization based on cloud top height (Price and Rind, 1992) with local scaling factors calculated from the Lightning Imaging Sensor (LIS) and Optical Transient Detector (OTD) satellite observa-

ACPD
15, 481–519, 2015

tions (Christian et al., 2003). Although the scaling approach is widely used to improve the representation of the global distribution of lightning, it carries some uncertainty as the future regions of lightning occurrence may differ from those currently observed (Murray et al., 2012).

Key reaction rates for the ozone budget were saved in every model grid cell, enabling chemistry to be analysed as a function of latitude, longitude, pressure and time. This approach was successfully used by Revell et al. (2012) to study stratospheric ozone chemistry. To better understand ozone transport, ozone tracers were implemented into SOCOL, based on the work of Grewe (2006) and Garny et al. (2011). Following this approach, the global ozone mixing ratio is disaggregated into 21 separate fields, according to in which of 21 predefined regions (defined by latitude and pressure) of the atmosphere the ozone originated; this approach is discussed further in Sect. 3.3.

To evaluate how realistically SOCOL simulates the distribution of tropospheric species, we compared ozone, CO and NO_2 (three key components of the tropospheric ozone budget) with satellite measurements over the period 2005–2009. Level 3 ozone and CO profile data were taken from TES (Tropospheric Emission Spectrometer), a Fourier transform infrared spectrometer onboard NASA's Aura satellite (e.g. Ho et al., 2009; Richards et al., 2008). Tropospheric NO_2 columns were compared with those measured by OMI (Ozone Monitoring Instrument) (Boersma et al., 2007).

2.2 Emission scenarios

SOCOL simulations were performed in support of the IGAC/SPARC Chemistry-Climate Model Initiative (CCMI; Eyring et al., 2013a), and therefore the boundary conditions used here adhere to the specifications of CCMI simulations, namely the REF-C2 and SEN-C2-*f*Emis simulations (hereafter *f*Emis, for brevity). These simulations are described in depth by Eyring et al. (2013a), but salient details are reproduced in Table 1. The REF-C2 simulation (1960–2100) was developed as a future reference simulation, to understand how the atmosphere would evolve under "best guess" estimates of future greenhouse gas concentrations, ozone-depleting substances (ODSs), ozone pre-

ACPD
15, 481–519, 2015

cursor emissions and sea-surface temperatures (SSTs). REF-C2 is based on RCP 6.0, a medium-high climate change scenario. Prescribed mixing ratios of greenhouse gases and long-lived chlorine, as well as emission fluxes of surface NO_x, NMVOCs and CO for the REF-C2 simulation are shown in Fig. 1. For biogenic isoprene, formaldehyde and other NMVOC emissions we use a climatology for the year 2000 (based on a MEGAN (Model of Emissions of Gases and Aerosols from Nature; Guenther et al. (2006)) run), while the biomass burning emissions follow those described by Lamarque et al. (2010) until 2000, and RCP 6.0 thereafter. Similarly, anthropogenic emissions of formaldehyde and other anthropogenic NMVOCs follow Lamarque et al. (2010) until 2000, then RCP 6.0.

The *f*Emis "fixed emissions" simulation (1960–2100) is identical to REF-C2, except that non-methane ozone precursor emissions are held constant at 1960 levels. For the present study, this simulation allowed us to explore the question of how global tropospheric ozone would evolve if air pollution remained at continuously low (1960) levels throughout the 21st century. Because methane is also an air pollutant but not fixed at 1960 levels in the *f*Emis simulation (as we are interested in its climate impact), we ran a short *f*CH_4 "fixed methane" simulation for 2080–2100. We chose this period of time because methane concentrations maximise under RCP 6.0 in the 2080s. The *f*CH_4 simulation used identical boundary conditions to the *f*Emis simulation, except methane concentrations were held constant at 1960 levels.

The REF-C2 and *f*Emis simulations were started in 1950, and the *f*CH_4 simulation was started in 2070, to allow ten years for the model to reach a steady state; this spin-up period was subsequently discarded and not used in our analyses.

ACPD
15, 481–519, 2015

3 Results and discussion

3.1 Evaluation of model performance

Model simulated ozone, CO and NO_2 fields from the SOCOL REF-C2 simulation were compared to satellite observations (Fig. 2). Ozone and CO profiles were taken from TES and NO_2 columns from OMI. Relative to TES, SOCOL has a large positive ozone bias of up to 30 ppb in the Northern Hemisphere and tropics, and a smaller negative bias (~ 5–10 ppb) in the Southern Hemisphere (Fig. 2a–c). One possibility for the large Northern Hemisphere bias might be a too-weak removal of NO_x from the troposphere, which is described by the HNO_3 washout process. In the model setup for the present study, a constant removal value was applied to the HNO_3 gas phase at each time step. Because HNO_3 can lead to ozone production when it is photolysed to form NO_2, recently obtained results suggest that a more realistic removal process for HNO_3 (based on in-cloud and below-cloud precipitation, and aerosol interaction (Chang, 1984; Seinfeld and Pandis, 2006)) indeed reduces SOCOL's overly large burden in the Northern Hemisphere. However, this is not pursued in the present study.

We note also that SOCOL is not alone among the current generation of models in overestimating northern midlatitude ozone. Small systematic high biases in the Northern Hemisphere and low biases in the Southern Hemisphere were also observed in the ACCMIP models (Bowman et al., 2013; Young et al., 2013). ACCMIP included a range of models, from coupled CCMs with comprehensive tropospheric and stratospheric chemistry, to chemistry transport models (CTMs) which do not calculate meteorology online, and CCMs with very simple tropospheric chemistry (Lamarque et al., 2013). Because the models used the same emissions (as each other, and as in the present study), it was concluded that "the prevalence of this bias could suggest they (the emissions) are deficient in some way, in either their amount or distribution, or both." (Young et al., 2013). It is not clear whether SOCOL's high ozone bias is a source issue (that is, emissions), a sink issue (HNO_3 washout), or a combination of the two, and this requires further investigation. However, similar to the ACCMIP models, SOCOL cor-

ACPD
15, 481–519, 2015

relates spatially very well with observations, despite biases in absolute ozone values; ozone concentrations are elevated in the Northern Hemisphere and over Africa compared with the Southern Hemisphere, and depleted ozone concentrations are seen over the tropical Pacific Ocean (discussed further in Sect. 3.2).

SOCOL simulates higher CO over regions where biomass burning is prevalent, namely South America, Africa and Indonesia, than observed by TES (Fig. 2d–f). Southern Hemisphere CO in SOCOL is in good agreement with TES, however in the Northern Hemisphere, CO is biased low by 20–40 ppb. The low Northern Hemisphere CO bias is linked with the high ozone bias in the same region, as ozone is the primary source of the OH radical, which in turn oxidises CO. Similar biases in CO were observed in the ACCMIP models; at 500 hPa, the multi-model mean is biased high compared with satellite observations over South America, Africa and Indonesia, and thought to be linked to biomass burning emissions (Naik et al., 2013). Furthermore, as seen in SOCOL, the multi-model mean is in good agreement with observations in the Southern Hemisphere.

SOCOL reproduces the elevated tropospheric NO_2 columns observed by OMI over North America, Europe and Asia, but overestimates their magnitude (Fig. 2g–i); this is linked in part to HNO_3 washout from the troposphere (as described above), and also to the general high ozone bias in SOCOL throughout the Northern Hemisphere, which is likely related to emissions. We note that potential discrepancies in emissions are a major source of uncertainty in our analyses. Indeed, Parrish et al. (2014) identify emissions as an issue in need of attention, given that CCMs consistently overestimate tropospheric ozone mixing ratios, and underestimate the magnitude of tropospheric ozone changes over the past 50–60 years.

Although SOCOL is subject to several biases in terms of absolute species concentrations, it captures the latitudinal and longitudinal distributions of ozone, CO and NO_2 convincingly. We now proceed to discuss the distribution of ozone in the 1960s, and the model-simulated changes until 2100.

ACPD
15, 481–519, 2015

3.2 Tropospheric ozone chemistry

Although tropospheric ozone chemistry is comprehensive and complex, we outline below some fundamental reaction cycles, as they are useful in discussing SOCOL's spatial ozone distribution later in this section. In the troposphere, ozone is produced via reaction cycles that begin with oxidation of a NMVOC or CO, as shown below:

$$\begin{aligned}
&CO + OH \rightarrow CO_2 + H\\
&H + O_2 + M \rightarrow HO_2 + M\\
&HO_2 + NO \rightarrow NO_2 + OH \qquad \text{(R1)}\\
&NO_2 + h\nu \rightarrow NO + O\\
&\underline{O + O_2 + M \rightarrow O_3 + M}\\
&CO + 2O_2 \rightarrow CO_2 + O_3
\end{aligned}$$

The reaction $HO_2 + NO$ is the rate-limiting step in ozone production and determines that the net effect of this cycle is ozone production. Other ozone producing cycles follow the oxidation of VOCs, such as methane, formaldehyde, or isoprene and its degradation products, leading to:

$$RO_2 + NO \rightarrow NO_2 + RO \qquad \text{(R2)}$$

where R represents the organic chain of the molecules RO_2 and RO.

In contrast, when air is NO_x-poor, rather than reacting with NO, as in the ozone production cycle (Reaction R1) above, the generated peroxy radicals HO_2 (and generally RO_2), will instead react with ozone, as in the cycles below, which are catalytic in HO_x, with ozone net loss rates R3 and R4:

$$\begin{aligned}
&CO + OH \rightarrow CO_2 + H\\
&H + O_2 + M \rightarrow HO_2 + M\\
&\underline{HO_2 + O_3 \rightarrow OH + 2O_2} \qquad \text{(R3)}\\
&CO + O_3 \rightarrow CO_2 + O_2
\end{aligned}$$

ACPD
15, 481–519, 2015

$$\begin{aligned} &OH + O_3 \rightarrow HO_2 + O_2 \\ &\underline{HO_2 + O_3 \rightarrow OH + 2O_2} \\ &2O_3 \rightarrow 3O_2 \end{aligned} \quad \text{(R4)}$$

In the tropics, where humidity and solar actinic fluxes are high, the following reaction mechanism (Reaction R5) can become the leading ozone loss reaction, even though it is not catalytic:

$$\begin{aligned} &O_3 + h\nu \rightarrow O(^1D) + O_2 \quad (\lambda < 320\,\text{nm}) \\ &\underline{O(^1D) + H_2O \rightarrow 2OH} \\ &O_3 + H_2O + h\nu \rightarrow O_2 + 2OH \end{aligned} \quad \text{(R5)}$$

In extremely NO_x-poor environments, ozone loss by Reaction (R5) can occur to such a large extent that minima in tropospheric ozone ensue, as in over the Amazon Basin and tropical Pacific Ocean in Fig. 3a. Minima in tropical Western Pacific ozone have been observed in a number of measurement campaigns (Kley et al., 1996; Singh et al., 1996; Tsutsumi et al., 2003; Rex et al., 2014). Furthermore, Rex et al. (2014) showed, using ozone and OH measurements in combination with the GEOS-Chem CTM, that very low tropospheric ozone and OH abundances exist in the tropical Western Pacific. Rex et al. (2014) explained that low OH abundances are concomitant with low ozone abundances in the tropical Western Pacific because ozone is the principal source of OH, and ozone loss via Reaction (R5) is so pronounced in this region. They also noted that low NO_x abundances further reduce OH because production of OH via $HO_2 + NO \rightarrow OH + NO_2$ becomes very slow (Gao et al., 2014). Results obtained from SOCOL largely support this hypothesis, except that the OH and ozone minima are located in different places (over Indonesia and over the Western Pacific Ocean, respectively). We suggest, therefore, that relatively high abundances of CO and VOCs from biomass burning are important for OH depletion, in combination with low NO_x abundances. The combination of high CO + VOCs and low NO_x drives ozone loss via Reactions (R3) and (R5), and suppresses ozone production via Reaction (R1). Be-

ACPD
15, 481–519, 2015

cause ozone abundances are so low over Indonesia, the HO_x partitioning from HO_2 into OH (via reaction of HO_2 with ozone) in Reaction (R3) becomes very slow, resulting in low modelled OH abundances (Fig. 3b).

Figure 3c and d shows the ratios of ozone production : loss, defined here as Reactions (R1 + R2)/(R3 + R4 + R5) and NO_x : NMVOCs + CO, respectively. We consider CO and NMVOCs together as they both undergo oxidation to initiate ozone production and destruction cycles. Here, NMVOCs are C_2–C_5 species that are related to isoprene, belonging to the reduced mechanism (MIM-1) outlined by Poeschl et al. (2000). One limitation of SOCOL is that the set of NMVOCs included is very small, namely formaldehyde, isoprene and the 15 other isoprene degradation products included in the MIM-1 isoprene oxidation mechanism. However, this subset of NMVOCs makes the mechanism detailed enough to accurately reproduce the diurnal cycle of important intermediate species like carbonyls, hydroperoxides and alkyl and peroxyl acyl nitrates, thus enabling the most relevant chemical processes for the tropospheric ozone budget to be represented (Poeschl et al., 2000). As shown in Fig. 3c and d, regions with high NO_x and low NMVOC + CO concentrations generally have high ozone production rates relative to ozone loss.

3.3 Projections for the 21st century

Given the projected changes in ozone precursor emissions, greenhouse gases and stratospheric ozone in the REF-C2 and *f*Emis simulations, how is tropospheric ozone projected to evolve through the 21st century? Further, are the projected changes dominated by changes in precursor emissions or by changes in climate? We focus our tropospheric analysis in the mid-troposphere, at 500 hPa. At this pressure the regional to hemispheric background ozone concentration is established, and the signal is representative for the surface, as seen when comparing Fig. 3a (ozone at 500 hPa) with Fig. 4 (surface ozone). Furthermore, most of the tropospheric ozone transport between low, middle and high latitudes happens in the mid-troposphere, as shown in Fig. 7.

ACPD
15, 481–519, 2015

500 hPa is also high enough in the atmosphere to be able to compare model output with satellite observations (Fig. 2).

Figure 5 shows the model-simulated free tropospheric concentrations of NO_x and NMVOCs + CO, as well as tropospheric and stratospheric ozone for the tropics and northern and southern midlatitudes. For the stratosphere, Fig. 5d shows that extratropical stratospheric column ozone is projected to increase through the 21st century in both the REF-C2 and *f*Emis simulations, owing to the phase-out of halocarbon gases under the Montreal Protocol for Substances that Deplete the Ozone Layer. Because of CO_2-induced cooling of the stratosphere (Bekki et al., 2011) and the increased rate of tropical upwelling (Avallone and Prather, 1996), the Northern and Southern Hemisphere stratospheric ozone columns increase to values slightly higher than those in 1980 by the end of the 21st century. Projected accelerated tropical upwelling is also expected to lead to slight decreases in tropical stratospheric ozone through the 21st century.

In the troposphere, the REF-C2 simulation shows that concentrations of NO_x, NMVOCs and CO increase dramatically through the late 20th century (Fig. 5a and b), but eventually start to decrease towards the end of the 21st century. Although anthropogenic NMVOC and CO emissions are fixed at 1960 levels in the *f*Emis simulation, an increase of CO still occurs as it is an oxidation product of CH_4, and CH_4 itself is not fixed at 1960 levels, but rather follows RCP 6.0 (Masui et al., 2011).

Global-mean tropospheric ozone increases substantially through the 20th century in the REF-C2 simulation, by 23 % until the 2020s, stays at these high values for about 40 years, and then decreases in the late 21st century (leading to an overall global-mean increase of 8 % between 1960 and 2100). The global-mean tropospheric ozone burden decreases by 1 % between 2000–2030, and 10 % between 2000–2100. These decreases are similar to the ensemble mean of the ACCMIP models which performed the RCP 6.0 simulation, of 1 and 9 % between 2000–2030 and 2000–2100, respectively (Young et al., 2013).

ACPD
15, 481–519, 2015

One seemingly inconsistent feature of Fig. 5 is that at northern midlatitudes, NO_x and NMVOC + CO concentrations decrease in the early 21st century, yet ozone concentrations in the REF-C2 simulation remain constant. To explain this feature, one must examine the spatial changes in ozone and its precursor emissions. Figure 6a and b shows that NO_x and NMVOC + CO both decrease in the Northern Hemisphere over Europe (and North America, in the case of NO_x). Therefore, ozone decreases by up to 4 % between the 2000s and 2020s over Europe (Fig. 6c). However, the decrease in NO_x of approximately 20 % over Europe and North America is compensated for by up to a 40 % increase in NO_x over Asia. In turn, this incurs an increase in ozone of up to 6 % in the same region, and, because of ozone's long lifetime in the troposphere, the increase extends as far as the west coast of North America. The decreases in ozone and its precursor emissions over Europe and North America and the increases over Asia are statistically significant at the 95 % level of confidence.

As shown in Fig. 6, changing regional emission patterns explain the substantial effect on northern midlatitude tropospheric ozone (Fig. 5c): by 1990, tropospheric ozone is 31 % higher than in 1960, and such high abundances are sustained until 2060. Attempts by Europe and North America to reduce emissions are partially offset by increases from Asia. It is well known that ozone formed from precursor emissions in Asia can be transported across the Pacific Ocean to the US, and this has previously been shown by, amongst others, Auvray et al. (2007), Derwent et al. (2008) and Zhang et al. (2010). Europe may also expect to be affected by increased emissions from other Northern Hemisphere sources in the early to mid-21st century; Auvray and Bey (2005) showed that Asian and North American sources of ozone contribute 8 and 11 % of the European annual ozone budget, respectively.

We further show decadal-mean ozone fluxes around the lower stratosphere and troposphere in Fig. 7. 15 of the 21 tracer regions are shown, with the remaining six regions located in the upper stratosphere above 30 hPa. Figure 7a quantifies ozone fluxes ($Tg\,yr^{-1}$) around the boundary layer (850–1000 hPa) and free troposphere (100–850 hPa between 30° N–30° S and 200–850 hPa elsewhere), ascent of air from the

ACPD
15, 481–519, 2015

tropics into the stratosphere, and downwelling from the stratosphere at extratropical latitudes, for the 1960s. Figure 7b shows the same plot for the 2050s, with increases of more than 20 % since the 1960s marked in red; this serves to highlight the increased export of ozone from tropical and northern midlatitude regions in the troposphere and boundary layer to surrounding regions (such as northern high latitudes), due to increased ozone production from precursor emissions in these regions between 1960–2050.

3.4 Ozone change with fixed precursor emissions

As shown in Fig. 5b, holding CO and NMVOC emissions constant at 1960 levels does not equate to constant concentrations of those species in the troposphere through the 21st century, because methane is an important source of CO and an ozone precursor in its own right (e.g., Seinfeld and Pandis, 2006), and methane is not held constant in the *f*Emis simulation. Figure 5c shows that in the absence of NO_x, the tropospheric ozone concentration maximises in the 2080s, which is approximately when methane concentrations maximise following RCP 6.0 (Fig. 1a).

To understand the effect on tropospheric ozone abundances if all ozone precursors, including methane, were held constant at 1960 levels, we ran an *f*Emis simulation with fixed methane (referred to as the fCH_4 simulation) for 2080–2100. Figure 5b shows that compared with 1960 of the *f*Emis and REF-C2 simulations, NMVOC + CO concentrations in the fCH_4 simulation are 5–10 ppb lower in the 2080s at northern midlatitudes and in the tropics, and decrease slightly at southern midlatitudes. Compared with 2080 of the *f*Emis and REF-C2 simulations, NMVOC + CO concentrations in the fCH4 simulation are significantly lower: in the global average, NMVOC + CO concentrations are 4 % lower in the *f*Emis simulation compared with the REF-C2, and 22 % lower in the fCH_4 simulation compared with the REF-C2. This corroborates the finding of Wang and Prinn (1999), that controlling methane emissions is more effective in controlling NMVOC + CO concentrations in the troposphere, than controlling NMVOC + CO emissions themselves.

ACPD
15, 481–519, 2015

Figure 5c shows that tropospheric ozone concentrations in the 2080s of the $f\mathrm{CH_4}$ simulation are approximately the same as in the 1960s. In the global mean, ozone in the $f\mathrm{CH_4}$ simulation is 16 % lower than in the REF-C2 simulation and 10 % lower than in the *f*Emis simulation. Methane has been shown to be an important ozone precursor historically, with both Shindell et al. (2009) and Lang et al. (2012) finding it to be responsible for most of the tropospheric ozone increase from pre-industrial to present times. Studies that have modelled projected tropospheric ozone under the different RCPs find methane to be the largest factor defining differences between the projections, because the RCPs assume huge reductions in $\mathrm{NO_x}$ and NMVOCs, but project growth in methane, especially in RCP 8.5 (Wild et al., 2012; Eyring et al., 2013b; Young et al., 2013).

3.5 Impacts of climate change and stratospheric ozone recovery

Although the *f*Emis simulation was designed to assess the impacts of climate change on atmosphere (Eyring et al., 2013a), there is a discrepancy with respect to methane's dual roles as a greenhouse gas and ozone precursor when it comes to analyzing tropospheric ozone, as discussed in the preceding section. However, given that ozone in the $f\mathrm{CH_4}$ simulation is the same in the 1960s and 2090s (Fig. 5c), this implies that the effects of climate change and stratospheric ozone recovery on ozone in the mid-troposphere are either negligible, or offset one another.

Climate change is thought to lead to tropospheric ozone decreases, due to increasing temperature and humidity, which accelerates the ozone destruction reactions (e.g. Toumi et al., 1996; Grewe et al., 2001; Doherty et al., 2013; Morgenstern et al., 2013). Figure 8a shows the ozone change at 500 hPa in the *f*Emis simulation between the 1960s and 2090s. The change is statistically significant at the 95 % confidence level almost everywhere. Here, with $\mathrm{NO_x}$, NMVOCs and CO fixed in the *f*Emis simulation, ozone increases up to 6 ppb almost everywhere (a global-mean increase of 6 %). The only exceptions are south of 50° S, where it remains unchanged and over the equatorial Pacific, where decreases of up to 2 ppb are seen. As discussed in Sect. 3.2, the

ACPD
15, 481–519, 2015

$H_2O + O(^1D)$ Reaction (R5) is very important for ozone loss over the remote tropical Pacific Ocean, and this reaction becomes faster over the period 1960–2100 as the troposphere becomes increasingly warm and humid (e.g. Zeng et al., 2010; Stevenson et al., 2013). Figure 8b shows the change in the ozone production : loss ratio (R1 + R2)/(R3 + R4 + R5) between the 1960s and 2090s. This ratio decreases everywhere due to the increased rate of ozone loss reactions, particularly at northern midlatitudes. Clearly temperature and humidity play an important role for ozone in the tropical Pacific (leading to less ozone), however ozone production resulting from the increase in methane is more important elsewhere, despite the increased rate of the ozone destruction reactions.

Alongside methane, two further factors contribute to the ozone increase in the *f*Emis simulation, although their influence is small: NO_x emissions from lightning, and STE. STE is projected to increase through the 21st century, because (a) as lower stratospheric ozone abundances increase, there is more ozone in the stratosphere available to be transported to the troposphere, and (b) the overall meridional circulation, the Brewer–Dobson circulation, is projected to strengthen (thus transporting more ozone from the stratosphere to the troposphere) (Hegglin and Shepherd, 2009; Zeng et al., 2010). Figure 8c shows the contribution of stratospheric ozone to the ozone budget at 500 hPa in the 1960s, calculated using the lower-stratospheric ozone tracers. The tracers define the lower stratosphere as the region between 30–200 hPa for 30–90° N and 30–90° S, and between 30–100 hPa for 30° N–30° S (Fig. 7), given that the tropopause sits at a lower pressure level in the tropics. In the 1960s, STE contributes between 0.1–5 % of ozone present at 500 hPa. We calculate a total flux from the lower stratosphere to the troposphere of 462 $Tg\,yr^{-1}$ in the 1960s. This is lower than the mean value from the model studies reviewed by Wild (2007) of 636 $Tg\,yr^{-1}$, but still within one standard deviation from their mean. Figure 8d shows the change in the contribution of stratospheric ozone to ozone at 500 hPa between the 1960s and 2090s in the *f*Emis simulation. STE contributes up to one additional ppb at southern midlatitudes, and this is statistically significant at the 95 % confidence level.

ACPD
15, 481–519, 2015

As discussed in Sect. 3.2, methane leads to ozone production in the presence of NO_x. Along with humidity and STE, lightning NO_x emissions may increase in a warmer climate, either due to increased frequency of thunderclouds (and therefore lightning), or more intense thunderstorms (Schumann and Huntrieser, 2007; Price, 2013). Figure 9a shows lightning NO_x emissions from SOCOL averaged over the 1960s, and shows that most lightning is produced over Africa and South America. Lightning NO_x emissions increase over the continents by 61 % between 1960–2100 (Fig. 9b), and by 48 % between 2000–2100. Banerjee et al. (2014) calculated increases in lightning NO_x emissions of 33 and 78 % between 2000–2100 in simulations using RCP 4.5 and RCP 8.5, respectively. Recalling that we used RCP 6.0, a 48 % increase over the same period is broadly consistent with their findings. However, the results also depend on the chosen lightning parameterization, which is coupled to the cloud top heights. Grewe (2009) showed that lightning NO_x emissions might also slightly decrease, when stronger but fewer convective events occur in a future climate. Although we cannot quantify any ozone increases induced by lightning NO_x emissions, they are likely to be small, and, together with STE, offset by the temperature-induced increased rates of ozone destruction reactions in the troposphere, similar to the findings of Morgenstern et al. (2013).

4 Conclusions

We have presented two CCM simulations covering the period 1960–2100, where the only factors differing in the model setup were the ozone precursor emissions (NO_x, NMVOCs and CO). The tropospheric extension to the SOCOL CCM is still new and with 17 NMVOCs only moderately sophisticated relative to some of the better-established tropospheric chemistry models, however the results presented here compare favorably with previous work.

In the REF-C2 simulation, which used RCP 6.0 greenhouse gases and ozone precursors, the maximum impact of ozone precursors on tropospheric ozone occurs between 1990 and 2060, when global-mean ozone in the free troposphere increases by 23 %

ACPD
15, 481–519, 2015

from 1960 levels. Although decreasing emissions of ozone precursor gases over Europe and North America lead to local reductions in ozone in the early 21st century, large increases in precursor gas emissions from Asia, combined with ozone's ability to be transported on inter-continental scales within the troposphere, lead to a 70 year period between 1990–2060 in which ozone abundances at northern midlatitudes are constantly elevated. In the late 21st century, reductions in ozone precursor gases, especially NO_x, lead to decreases in tropospheric ozone globally. However, global-mean concentrations are still 8 % higher in the 2090s compared with the 1960s.

In the *f*Emis (fixed ozone precursor emissions) simulation, global-mean ozone increases by 6 % between 1960–2100, mostly because methane concentrations were not held constant. A short sensitivity simulation for 2080–2100 with all ozone precursors (including methane) held constant shows that tropospheric ozone concentrations are the same as in 1960. Increased flux of ozone from the stratosphere to the troposphere, and increased emissions of NO_x from lightning in a warmer climate contribute to increases in tropospheric ozone through the 21st century, although their effects are relatively small. Other climate-change related factors we have not examined include biogenic emissions, which are thought to increase with temperature, but are not considered in our simulations because SOCOL does not include an interactive scheme for biogenic emissions. Notably, we have considered only a single climate change scenario (RCP 6.0), and the impacts of climate change will differ under different climate scenarios. We furthermore reiterate that emissions of ozone precursor gases are also a significant source of uncertainty in our results.

Overall, and given the assumptions inherent in the climate and ozone precursor emissions scenarios we used, anthropogenic NO_x emissions have the largest influence on tropospheric ozone in our simulations. Methane has the second largest influence, which is approximately one-third that of anthropogenic NO_x emissions. We therefore conclude that emission policies globally have the largest role to play in determining tropospheric ozone evolution through the 21st century.

ACPD
15, 481–519, 2015

Acknowledgements. LER is supported under the ETH Zurich Postdoctoral Fellowship Program. AC and AS are supported by the Competence Center Environment and Sustainability (CCES) under the project MAIOLICA-2. AS is furthermore supported by the SNSF under grant no. 200021_138037/1 (FuMES). FT is supported by a SNSF post-doctoral grant. We acknowledge the free use of tropospheric NO_2 column data from the OMI sensor from www.temis.nl.

References

Auvray, M. and Bey, I.: Long-range transport to Europe: seasonal variations and implications for the European ozone budget, J. Geophys. Res., 110, D11303, doi:10.1029/2004JD005503, 2005.

Auvray, M., Bey, I., Llull, E., Schultz, M. G., and Rast, S.: A model investigation of tropospheric ozone chemical tendencies in long-range transported pollution plumes, J. Geophys. Res., 112, D05304, doi:10.1029/2006JD007137, 2007.

Avallone, L. M. and Prather, M. J.: Photochemical evolution of ozone in the lower tropical stratosphere, J. Geophys. Res., 101, 1457–1461, doi:10.1029/95JD03010, 1996.

Banerjee, A., Archibald, A. T., Maycock, A. C., Telford, P., Abraham, N. L., Yang, X., Braesicke, P., and Pyle, J. A.: Lightning NO_x, a key chemistry–climate interaction: impacts of future climate change and consequences for tropospheric oxidising capacity, Atmos. Chem. Phys., 14, 9871–9881, doi:10.5194/acp-14-9871-2014, 2014.

Bekki, S., Bodeker, G. E. (Coordinating Lead Authors), Bais, A. F., Butchart, N., Eyring, V., Fahey, D. W., Kinnison, D. E., Langematz, U., Mayer, B., Portmann, R. W., Rozanov, E., Braesicke, P., Charlton-Perez, A. J., Chubarova, N. E., Cionni, I., Diaz, S. B., Gillett, N. P., Giorgetta, M. A., Komala, N., Lefèvre, F., McLandress, C., Perlwitz, J., Peter, T., and Shibata, K.: Future ozone and its impact on surface UV, chapter 3 in: Scientific Assessment of Ozone Depletion: 2010, Global Ozone Research and Monitoring Project – Report No. 52, 516 pp, World Meteorological Organization, Geneva, Switzerland, 2011.

Boersma, K. F., Eskes, H. J., Veefkind, J. P., Brinksma, E. J., van der A, R. J., Sneep, M., van den Oord, G. H. J., Levelt, P. F., Stammes, P., Gleason, J. F., and Bucsela, E. J.: Near-real time retrieval of tropospheric NO_2 from OMI, Atmos. Chem. Phys., 7, 2103–2118, doi:10.5194/acp-7-2103-2007, 2007.

ACPD
15, 481–519, 2015

Bowman, K. W., Shindell, D. T., Worden, H. M., Lamarque, J.F., Young, P. J., Stevenson, D. S., Qu, Z., de la Torre, M., Bergmann, D., Cameron-Smith, P. J., Collins, W. J., Doherty, R., Dalsøren, S. B., Faluvegi, G., Folberth, G., Horowitz, L. W., Josse, B. M., Lee, Y. H., MacKenzie, I. A., Myhre, G., Nagashima, T., Naik, V., Plummer, D. A., Rumbold, S. T., Skeie, R. B., Strode, S. A., Sudo, K., Szopa, S., Voulgarakis, A., Zeng, G., Kulawik, S. S., Aghedo, A. M., and Worden, J. R.: Evaluation of ACCMIP outgoing longwave radiation from tropospheric ozone using TES satellite observations, Atmos. Chem. Phys., 13, 4057–4072, doi:10.5194/acp-13-4057-2013, 2013.

Butchart, N., Cionni, I., Eyring, V., Shepherd, T. G., Waugh, D. W., Akiyoshi, H., Austin, J., Brühl, C., Chipperfield, M. P., Cordero, E., Dameris, M., Deckert, R., Dhomse, S., Frith, S. M., Garcia, R. R., Gettelman, A., Giorgetta, M. A., Kinnison, D. E., Li, F., Mancini, E., McLandress, C., Pawson, S., Pitari, G., Plummer, D. A., Rozanov, E., Sassi, F., Scinocca, J. F., Shibata, K., Steil, B., and Tian, W.: Chemistry-climate model simulations of twenty-first century stratospheric climate and circulation changes, J. Climate, 23, 5349–5374, doi:10.1175/2010JCLI3404.1, 2010.

Chang, J. S., Brost, R. A., Isaksen, I. S. A., Madronich, S., Middleton, P., Stockwell, W. R., and Walcek, C. J.: A three-dimensional Eulerian acid deposition model: physical concepts and formulation, J. Geophys. Res., 92, 14681–14700, doi:10.1029/JD092iD12p14681, 1987.

Chang, T. Y.: Rain and snow scavenging of HNO_3 vapor in the atmosphere, Atmos. Environ., 18, 191–197, doi:10.1016/0004-6981(84)90242-7, 1984.

Christian, H. J., Blakeslee, R. J., Boccippio, D. J., Boeck, W. L., Buechler, D. E., Driscoll, K. T., Goodman, S. J., Hall, J. M., Koshak, W. J., Mach, D. M., and Stewart, M. F.: Global frequency and distribution of lightning as observed from space by the Optical Transient Detector, J. Geophys. Res., 108, doi:10.1029/2002JD002347, 2003.

Denman, K. L., Brasseur, G., Chidthaisong, A., Ciais, P., Cox, P. M., Dickinson, R. E., Hauglustaine, D., Heinze, C., Holland, E., Jacob, D., Lohmann, U., Ramachandran, S., da Silva Dias, P. L., Wofsy, S. C., and Zhang, X.: Couplings between changes in the climate system and biogeochemistry, chapter 7, in: Climate Change 2007: the Physical Science Basis. Contribution of Working Group I to the Fourth Assessment Report of the Intergovernmental Panel on Climate Change, edited by: Solomon, S., Qin, D., Manning, M., Chen, Z., Marquis, M., Averyt, K. B., Tignor, M., and Miller, H. L., Cambridge University Press, Cambridge, UK, New York, NY, USA, 547–550, 2007.

ACPD
15, 481–519, 2015

Derwent, R. G., Stevenson, D. S., Doherty, R. M., Collins, W. J., and Sanderson, M. G.: How is surface ozone in Europe linked to Asian and North American NO_x emissions?, Atmos. Environ., 42, 7412–7422, doi:10.1016/j.atmosenv.2008.06.037, 2008.

Doherty, R. M., Wild, O., Shindell, D. T., Zeng, G., MacKenzie, I. A., Collins, W. J., Fiore, A. M., Stevenson, D. S., Dentener, F. J., Schultz, M. G., Hess, P., Derwent, R. G., and Keating, T. J.: Impacts of climate change on surface ozone and intercontinental ozone pollution: a multi-model study, J. Geophys. Res., 118, 3744–3763, doi:10.1002/jgrd.50266, 2013.

Egorova, T. A., Rozanov, E. V., Zubov, V. A., and Karol, I. L.: Model for investigating ozone trends (MEZON), Izv. Atmos. Ocean. Phy., 39, 277–292, 2003.

Eyring, V., Lamarque, J.-F., Hess, P., Arfeuille, F., Bowman, K., Chipperfield, M. P., Duncan, B., Fiore, A., Gettelman, A., Giorgetta, M. A., Granier, C., Hegglin, M., Kinnison, D., Kunze, M., Langematz, U., Luo, B., Martin, R., Matthes, K., Newman, P. A., Peter, T., Robock, A., Ryerson, T., Saiz-Lopez, A., Salawitch, R., Schultz, M., Shepherd, T. G., Shindell, D., Staehelin, J., Tegtmeier, S., Thomason, L., Tilmes, S., Vernier, J.-P., Waugh, D. W., and Young, P. J.: Overview of IGAC/SPARC Chemistry-Climate Model Initiative (CCMI) Community Simulations in Support of Upcoming Ozone and Climate Assessments, SPARC Newsletter no. 40, ISSN 1245–4680, 48–66, 2013a.

Eyring, V., Arblaster, J. M., Cionni, I., Sedláček, J., Perlwitz, J., Young, P. J., Bekki, S., Bergmann, D., Cameron-Smith, P., Collins, W. J., Faluvegi, G., Gottschaldt, K.-D., Horowitz, L. W., Kinnison, D. E., Lamarque, J.-F., Marsh, D. R., Saint-Martin, D., Shindell, D. T., Sudo, K., Szopa, S., and Watanabe, S.: Long-term ozone changes and associated climate impacts in CMIP5 simulations, J. Geophys. Res., 118, 5029–5060, doi:10.1002/jgrd.50316, 2013b.

Forster, P., Ramaswamy, V., Artaxo, P., Berntsen, T., Betts, R., Fahey, D. W., Haywood, J., Lean, J., Lowe, D. C., Myhre, G., Nganga, J., Prinn, R., Raga, G., Schulz, M., and van Dorland, R.: Changes in atmospheric constituents and in radiative forcing, chapter 2, in: Climate Change 2007: the Physical Science Basis. Contribution of Working Group I to the Fourth Assessment Report of the Intergovernmental Panel on Climate Change, edited by: Solomon, S., Qin, D., Manning, M., Chen, Z., Marquis, M., Averyt, K. B., Tignor, M., and Miller, H. L., Cambridge University Press, Cambridge, UK, New York, NY, USA, 150–152, 2007.

ACPD
15, 481–519, 2015

Gao, R. S., Rosenlof, K. H., Fahey, D. W., Wennberg, P. O., Hintsa, E. J., and Hanisco, T. F.: OH in the tropical upper troposphere and its relationships to solar radiation and reactive nitrogen, J. Atmos. Chem., 71, 55–64, doi:10.1007/s10874-014-9280-2, 2014.

Garny, H., Grewe, V., Dameris, M., Bodeker, G. E., and Stenke, A.: Attribution of ozone changes to dynamical and chemical processes in CCMs and CTMs, Geosci. Model Dev., 4, 271–286, doi:10.5194/gmd-4-271-2011, 2011.

Grewe, V.: The origin of ozone, Atmos. Chem. Phys., 6, 1495–1511, doi:10.5194/acp-6-1495-2006, 2006.

Grewe, V.: Impact of lightning on air chemistry and climate, in: Lightning: Principles, Instruments and Applications Review of Modern Lightning Research, edited by: Betz, H. D., Schumann, U., and Laroche, P., Springer Verlag, 524–551, 2009.

Grewe, V., Dameris, M., Hein, R., Sausen, R., and Steil, B.: Future changes of the atmospheric composition and the impact of climate change, Tellus B, 53, 103–121, 2001.

Guenther, A., Karl, T., Harley, P., Wiedinmyer, C., Palmer, P. I., and Geron, C.: Estimates of global terrestrial isoprene emissions using MEGAN (Model of Emissions of Gases and Aerosols from Nature), Atmos. Chem. Phys., 6, 3181–3210, doi:10.5194/acp-6-3181-2006, 2006.

Hegglin, M. I. and Shepherd, T. G.: Large climate-induced changes in ultraviolet index and stratosphere-to-troposphere ozone flux, Nat. Geosci., 2, 687–691, doi:10.1038/ngeo604, 2009.

Ho, S., Edwards, D. P., Gille, J. C., Luo, M., Osterman, G. B., Kulawik, S. S., and Worden, H.: A global comparison of carbon monoxide profiles and column amounts from Tropospheric Emission Spectrometer (TES) and Measurements of Pollution in the Troposphere (MOPITT), J. Geophys. Res., 114, D21307, doi:10.1029/2009JD012242, 2009.

Kley, D., Crutzen, P. J., Smit, H. G. J., Vömel, H., Oltmans, S. J., Grassl, H., and Ramanathan, V.: Observations of near-zero ozone concentrations over the convective Pacific: effects on air chemistry, Science, 274, 230–233, doi:10.1126/science.274.5285.230, 1996.

Lamarque, J.-F., Bond, T. C., Eyring, V., Granier, C., Heil, A., Klimont, Z., Lee, D., Liousse, C., Mieville, A., Owen, B., Schultz, M. G., Shindell, D., Smith, S. J., Stehfest, E., Van Aardenne, J., Cooper, O. R., Kainuma, M., Mahowald, N., McConnell, J. R., Naik, V., Riahi, K., and van Vuuren, D. P.: Historical (1850–2000) gridded anthropogenic and biomass burning emissions of reactive gases and aerosols: methodology and application, Atmos. Chem. Phys., 10, 7017–7039, doi:10.5194/acp-10-7017-2010, 2010.

ACPD
15, 481–519, 2015

Lamarque, J.-F., Shindell, D. T., Josse, B., Young, P. J., Cionni, I., Eyring, V., Bergmann, D., Cameron-Smith, P., Collins, W. J., Doherty, R., Dalsoren, S., Faluvegi, G., Folberth, G., Ghan, S. J., Horowitz, L. W., Lee, Y. H., MacKenzie, I. A., Nagashima, T., Naik, V., Plummer, D., Righi, M., Rumbold, S. T., Schulz, M., Skeie, R. B., Stevenson, D. S., Strode, S., Sudo, K., Szopa, S., Voulgarakis, A., and Zeng, G.: The Atmospheric Chemistry and Climate Model Intercomparison Project (ACCMIP): overview and description of models, simulations and climate diagnostics, Geosci. Model Dev., 6, 179–206, doi:10.5194/gmd-6-179-2013, 2013.

Lang, C., Waugh, D. W., Olsen, M. A., Douglass, A. R., Liang, Q., Nielsen, J. E., Oman, L. D., Pawson, S., and Stolarski, R. S.: The impact of greenhouse gases on past changes in tropospheric ozone, J. Geophys. Res., 117, doi:10.1029/2012JD018293, 2012.

Lin, S. J. and Rood, R. B.: Multidimensional flux-form semi-Lagrangian transport schemes, Mon. Weather Rev., 124, 2046–2070, doi:10.1175/1520-0493(1996)124<2046:MFFSLT>2.0.CO;2, 1996.

Masui, T., Matsumoto, K., Hijioka, Y., Kinoshita, T., Nozawa, T., Ishiwatari, S., Kato, E., Shukla, P. R., Yamagata, Y., and Kainuma, M.: An emission pathway for stabilization at 6 $W m^{-2}$ radiative forcing, Climatic Change, 109, 59–76, doi:10.1007/s10584-011-0150-5, 2011.

Meehl, G. A., Washington, W. M., Arblaster, J. M., Hu, A., Teng, H., Kay, J. E., Gettelman, A., Lawrence, D. M., Sanderson, B. M., and Strand, W. G.: Climate change projections in CESM1(CAM5) compared to CCSM4, J. Climate, 26, 6287–6308, doi:10.1175/JCLI-D-12-00572.1, 2013.

Morgenstern, O., Zeng, G., Abraham, N. L., Telford, P. J., Braesicke, P., Pyle, J. A., Hardiman, S. C., O'Connor, F. M., and Johnson, C. E.: Impacts of climate change, ozone recovery, and increasing methane on surface ozone and the tropospheric oxidizing capacity, J. Geophys. Res., 118, 1028–1041, doi:10.1029/2012JD018382, 2013.

Murray, L. T., Jacob, D. J., Logan, J. A., Hudman, R. C., and Koshak, W. J.: Optimized regional and interannual variability of lightning in a global chemical transport model constrained by LIS/OTD satellite data, J. Geophys. Res., 117, D20307, doi:10.1029/2012jd017934, 2012.

Naik, V., Voulgarakis, A., Fiore, A. M., Horowitz, L. W., Lamarque, J.-F., Lin, M., Prather, M. J., Young, P. J., Bergmann, D., Cameron-Smith, P. J., Cionni, I., Collins, W. J., Dalsøren, S. B., Doherty, R., Eyring, V., Faluvegi, G., Folberth, G. A., Josse, B., Lee, Y. H., MacKenzie, I. A., Nagashima, T., van Noije, T. P. C., Plummer, D. A., Righi, M., Rumbold, S. T., Skeie, R.,

ACPD
15, 481–519, 2015

Shindell, D. T., Stevenson, D. S., Strode, S., Sudo, K., Szopa, S., and Zeng, G.: Preindustrial to present-day changes in tropospheric hydroxyl radical and methane lifetime from the Atmospheric Chemistry and Climate Model Intercomparison Project (ACCMIP), Atmos. Chem. Phys., 13, 5277–5298, doi:10.5194/acp-13-5277-2013, 2013.

Parrish, D. D., Lamarque, J.-F., Naik, V., Horowitz, L. Shindell, D. T., Staehelin, J., Derwent, R., Cooper, O. R., Tanimoto, H., Volz-Thomas, A., Gilge, S., Scheel, H.-E., Steinbacher, M., and Fröhlich, M.: Long-term changes in lower tropospheric baseline ozone concentrations: comparing chemistry-climate models and observations at northern midlatitudes, J. Geophys. Res., 119, 5719–5736, doi:10.1002/2013JD021435, 2014.

Poeschl, U., von Kuhlmann, R., Poisson, N., and Crutzen, P. J.: Development and intercomparison of condensed isoprene oxidation mechanisms for global atmospheric modeling, J. Atmos. Chem., 37, 29–52, doi:10.1023/A:1006391009798, 2000.

Price, C. and Rind, D.: A simple lightning parameterization for calculating global lightning distributions, J. Geophys. Res., 97, 9919–9933, doi:10.1029/92JD00719, 1992.

Price, C. G.: Lightning applications in weather and climate research, Surv. Geophys., 34, 755–767, doi:10.1007/s10712-012-9218-7, 2013.

Rayner, N. A., Parker, D. E., Horton, E. B., Folland, C. K., Alexander, L. V., Rowell, D. P., Kent, E. C., and Kaplan, A.: Global analyses of sea surface temperature, sea ice, and night marine air temperature since the late nineteenth century, J. Geophys. Res., 108, 4407, doi:10.1029/2002JD002670, 2003.

Revell, L. E., Bodeker, G. E., Smale, D., Lehmann, R., Huck, P. E., Williamson, B. E., Rozanov, E., and Struthers, H.: The effectiveness of N_2O in depleting stratospheric ozone, Geophys. Res. Lett., 39, L15806, doi:10.1029/2012GL052143, 2012.

Rex, M., Wohltmann, I., Ridder, T., Lehmann, R., Rosenlof, K., Wennberg, P., Weisenstein, D., Notholt, J., Krüger, K., Mohr, V., and Tegtmeier, S.: A tropical West Pacific OH minimum and implications for stratospheric composition, Atmos. Chem. Phys., 14, 4827–4841, doi:10.5194/acp-14-4827-2014, 2014.

Richards, N. A. D., Osterman, G. B., Browell, E. V., Hair, J. W., Avery, M., and Li, Q.: Validation of Tropospheric Emission Spectrometer ozone profiles with aircraft observations during the Intercontinental Chemical Transport Experiment-B, J. Geophys. Res., 113, D16S29, doi:10.1029/2007JD008815, 2008.

Roeckner, E., Bäuml, G., Bonaventura, L., Brokopf, R., Esch, M., Giorgetta, M., Hagemann, S., Kirchner, I., Kornblueh, L., Manzini, E., Rhodin, A., Schlese, U., Schulzweida, U., and

ACPD
15, 481–519, 2015

Tompkins, A.: The atmospheric general circulation model ECHAM 5. Part I: Model description, Max-Planck-Institut für Meteorologie, Hamburg, Report No. 349, available at: http://www.mpimet.mpg.de/fileadmin/publikationen/Reports/max_scirep_349.pdf, 2003.

Rozanov, E., Schlesinger, M. E., Zubov, V., Yang, F., and Andronova, N. G.: The UIUC three-dimensional stratospheric chemical transport model: description and evaluation of the simulated source gases and ozone, J. Geophys. Res., 104, 11755–11781, 1999.

Schumann, U. and Huntrieser, H.: The global lightning-induced nitrogen oxides source, Atmos. Chem. Phys., 7, 3823–3907, doi:10.5194/acp-7-3823-2007, 2007.

Seinfeld, J. H. and Pandis, S. N.: Atmospheric Chemistry and Physics: from Air Pollution to Climate Change, 2nd edn., John Wiley and Sons, Inc., Hoboken, New Jersey, USA, 2006.

Shindell, D. T., Faluvegi, G., Koch, D. M., Schmidt, G. A., Unger, N., and Bauer, S. E.: Improved attribution of climate forcing to emissions, Science, 326, 716–718, doi:10.1126/science.1174760, 2009.

Silva, R. A., West, J. J., Zhang, Y., Anenberg, S. C., Lamarque, J.-F., Shindell, D. T., Collins, W. J., Dalsoren, S., Faluvegi, G., Folberth, G., Horowitz, L. W., Nagashima, T., Naik, V., Rumbold, S., Skeie, R., Sudo, K., Takemura, T., Bergmann, D., Cameron-Smith, P., Cionni, I., Doherty, R. M., Eyring, V., Josse, B., MacKenzie, I. A., Plummer, D., Righi, M., Stevenson, D. S., Strode, S., Szopa, S., and Zeng, G.: Global premature mortality due to anthropogenic outdoor air pollution and the contribution of past climate change, Environ. Res. Lett., 8, 034005, doi:10.1088/1748-9326/8/3/034005, 2013.

Singh, H. B., Gregory, G. L., Anderson, B., Browell, E., Sachse, G. W., Davis, D. D., Crawford, J., Bradshaw, J. D., Talbot, R., Blake, D. R., Thornton, D., Newell, R., and Merrill, J.: Low ozone in the marine boundary layer of the tropical Pacific Ocean: photochemical loss, chlorine atoms, and entrainment, J. Geophys. Res., 101, 1907–1917, doi:10.1029/95JD01028, 1996.

SPARC CCMVal: SPARC Report on the Evaluation of Chemistry-Climate Models, edited by: Eyring, V., Shepherd, T. G., and Waugh, D. W., SPARC Report No. 5, WCRP-132, WMO/TD-No. 1526, available at: http://www.sparc-climate.org/publications/sparc-reports/sparc-report-no5/, 2010.

Stenke, A., Schraner, M., Rozanov, E., Egorova, T., Luo, B., and Peter, T.: The SOCOL version 3.0 chemistry–climate model: description, evaluation, and implications from an advanced transport algorithm, Geosci. Model Dev., 6, 1407–1427, doi:10.5194/gmd-6-1407-2013, 2013.

ACPD
15, 481–519, 2015

Stevenson, D. S., Young, P. J., Naik, V., Lamarque, J.-F., Shindell, D. T., Voulgarakis, A., Skeie, R. B., Dalsoren, S. B., Myhre, G., Berntsen, T. K., Folberth, G. A., Rumbold, S. T., Collins, W. J., MacKenzie, I. A., Doherty, R. M., Zeng, G., van Noije, T. P. C., Strunk, A., Bergmann, D., Cameron-Smith, P., Plummer, D. A., Strode, S. A., Horowitz, L., Lee, Y. H., Szopa, S., Sudo, K., Nagashima, T., Josse, B., Cionni, I., Righi, M., Eyring, V., Conley, A., Bowman, K. W., Wild, O., and Archibald, A.: Tropospheric ozone changes, radiative forcing and attribution to emissions in the Atmospheric Chemistry and Climate Model Intercomparison Project (ACCMIP), Atmos. Chem. Phys., 13, 3063–3085, doi:10.5194/acp-13-3063-2013, 2013.

Thompson, A. M.: The oxidizing capacity of the Earth's atmosphere – probable past and future changes, Science, 256, 1157–1165, doi:10.1126/science.256.5060.1157, 1992.

Toumi, R., Haigh, J. D., and Law, K. S.: A tropospheric ozone-lightning climate feedback, Geophys. Res. Lett., 23, 1037–1040, 1996.

Tsutsumi, Y., Makino, Y., and Jensen, J. B.: Vertical and latitudinal distributions of tropospheric ozone over the western Pacific: case studies from the PACE aircraft missions, J. Geophys. Res., 108, doi:10.1029/2001JD001374, 2003.

Wang, C. and Prinn, G.: Impact of emissions, chemistry and climate on atmospheric carbon monoxide: 100-year predictions from a global chemistry-climate model, Chemosphere, 1, 73–81, 1999.

West, J. J., Szopa, S., and Hauglustaine, D. A.: Human mortality effects of future concentrations of tropospheric ozone, C. R. Geosci., 339, 775–783, doi:10.1016/j.crte.2007.08.005, 2007.

Wild, O.: Modelling the global tropospheric ozone budget: exploring the variability in current models, Atmos. Chem. Phys., 7, 2643–2660, doi:10.5194/acp-7-2643-2007, 2007.

Wild, O., Fiore, A. M., Shindell, D. T., Doherty, R. M., Collins, W. J., Dentener, F. J., Schultz, M. G., Gong, S., MacKenzie, I. A., Zeng, G., Hess, P., Duncan, B. N., Bergmann, D. J., Szopa, S., Jonson, J. E., Keating, T. J., and Zuber, A.: Modelling future changes in surface ozone: a parameterized approach, Atmos. Chem. Phys., 12, 2037–2054, doi:10.5194/acp-12-2037-2012, 2012.

World Meteorological Organization: Scientific Assessment of Ozone Depletion: 2010, WMO Global Ozone Research and Monitoring Project – Report No. 52, Geneva, Switzerland, 2011.

Young, P. J., Archibald, A. T., Bowman, K. W., Lamarque, J.-F., Naik, V., Stevenson, D. S., Tilmes, S., Voulgarakis, A., Wild, O., Bergmann, D., Cameron-Smith, P., Cionni, I.,

ACPD
15, 481–519, 2015

Collins, W. J., Dalsøren, S. B., Doherty, R. M., Eyring, V., Faluvegi, G., Horowitz, L. W., Josse, B., Lee, Y. H., MacKenzie, I. A., Nagashima, T., Plummer, D. A., Righi, M., Rumbold, S. T., Skeie, R. B., Shindell, D. T., Strode, S. A., Sudo, K., Szopa, S., and Zeng, G.: Pre-industrial to end 21st century projections of tropospheric ozone from the Atmospheric Chemistry and Climate Model Intercomparison Project (ACCMIP), Atmos. Chem. Phys., 13, 2063–2090, doi:10.5194/acp-13-2063-2013, 2013.

Zeng., G., Morgenstern, O., Braesicke, P., and Pyle, J. A.: Impact of stratospheric ozone recovery on tropospheric ozone and its budget, Geophys. Res. Lett., 37, L09805, doi:10.1029/2010GL042812, 2010.

Zhang, H., Wu, S., Huang, Y., and Wang, Y.: Effects of stratospheric ozone recovery on photochemistry and ozone air quality in the troposphere, Atmos. Chem. Phys., 14, 4079–4086, doi:10.5194/acp-14-4079-2014, 2014.

Zhang, Y., Olsen, S. C., Dubey, M. K.: WRF/Chem simulated springtime impact of rising Asian emissions on air quality over the U. S., Atmos. Environ., 44, 2799–2812, doi:10.1016/j.atmosenv.2010.05.003, 2010.

Zubov, V., Rozanov, E., and Schleisinger, M. E.: Hybrid scheme for three-dimensional advective transport, Mon. Weather Rev., 127, 1335–1346, 1999.

ACPD
15, 481–519, 2015

Table 1. Summary of boundary conditions used for the SOCOL CCM simulations.

	REF-C2 (1960–2100)	*f*Emis (1960–2100)	*f*CH_4 (2080–2100)
Greenhouse gases (CO_2, N_2O, CH_4)	Observations until 2005 then RCP 6.0 (Masui et al., 2011)	Same as REF-C2	CO_2 and N_2O same as REF-C2; CH_4 fixed at 1960 levels
Ozone and aerosol precursor emissions	Observations until 2000 (Lamarque et al., 2010), then RCP 6.0	Fixed at 1960 levels	Fixed at 1960 levels
SSTs	Observations until 2005 (Rayner et al., 2003), then RCP 6.0 (Meehl et al., 2013)	Same as REF-C2	Same as REF-C2
ODSs	Observations + the A1 scenario from WMO (2011)	Same as REF-C2.	Same as REF-C2

ACPD
15, 481–519, 2015

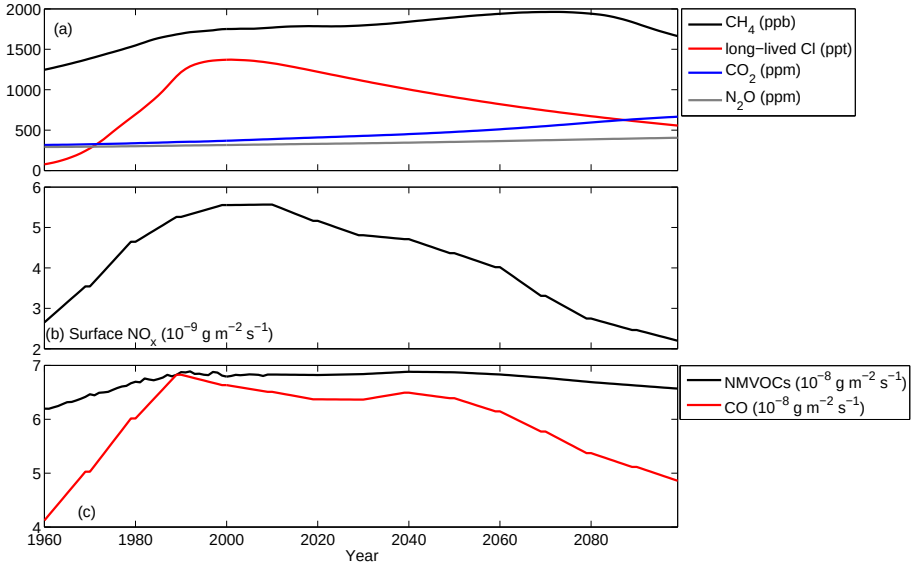

Figure 1. Boundary conditions used in the REF-C2 simulation. **(a)** CO_2, CH_4, N_2O mixing ratios following RCP 6.0, and long-lived chlorine mixing ratios following the WMO A1 scenario for ODSs. **(b)** Surface NO_x emission fluxes, following RCP 6.0. **(c)** Surface CO and NMVOC emission fluxes, following RCP 6.0.

ACPD
15, 481–519, 2015

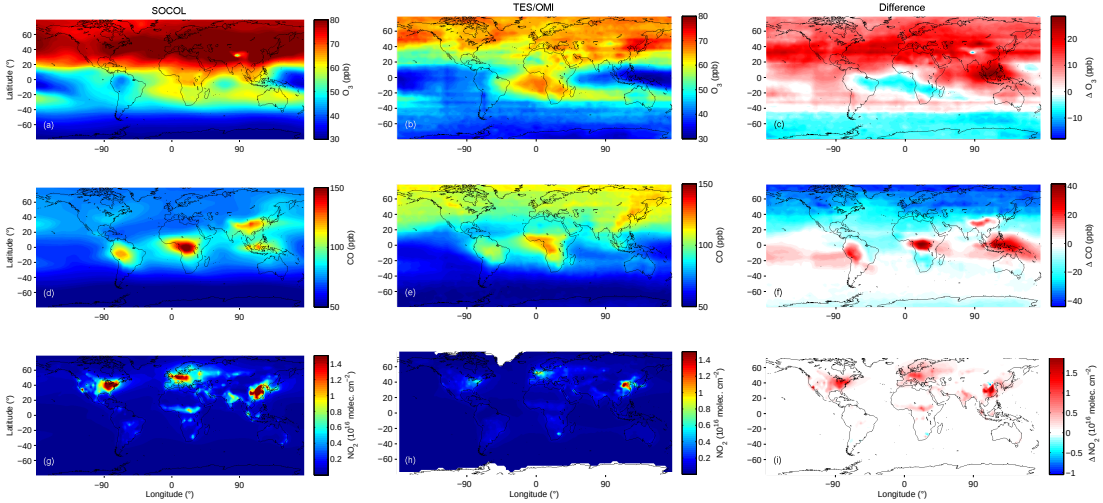

Figure 2. Comparisons of SOCOL model results (from the REF-C2 simulation) with observations, averaged over 2005–2009, for: **(a)** SOCOL ozone, 500 hPa; **(b)** TES ozone, 464 hPa; **(c)** ozone difference (**a** minus **b**); **(d)** SOCOL CO, 500 hPa; **(e)** TES CO, 464 hPa; **(f)** CO difference (**d** minus **e**); **(g)** SOCOL tropospheric column NO_2; **(h)** OMI tropospheric column NO_2; **(i)** NO_2 difference (**g** minus **h**).

ACPD
15, 481–519, 2015

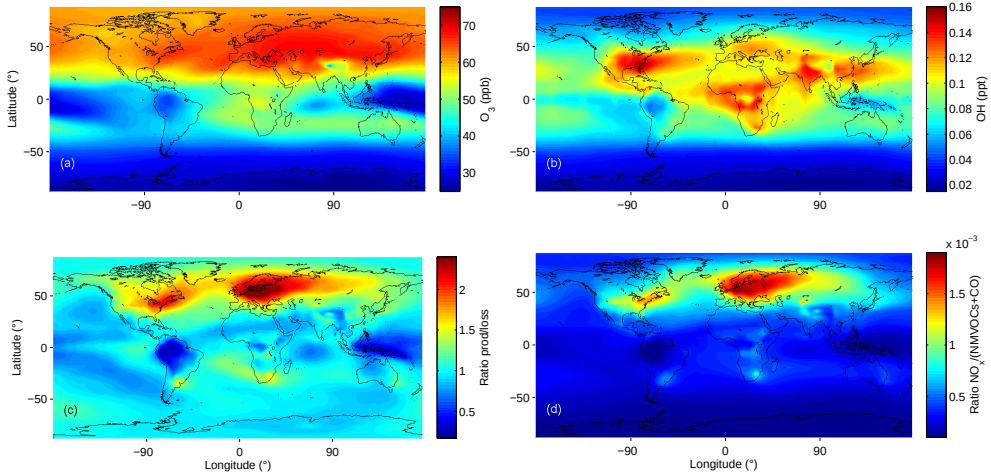

Figure 3. Results from the REF-C2 simulation, 1960–1969 average, 500 hPa. **(a)** Ozone; **(b)** OH; **(c)** ratio of ozone production over loss; **(d)** ratio of NO_x : NMVOCs + CO.

ACPD
15, 481–519, 2015

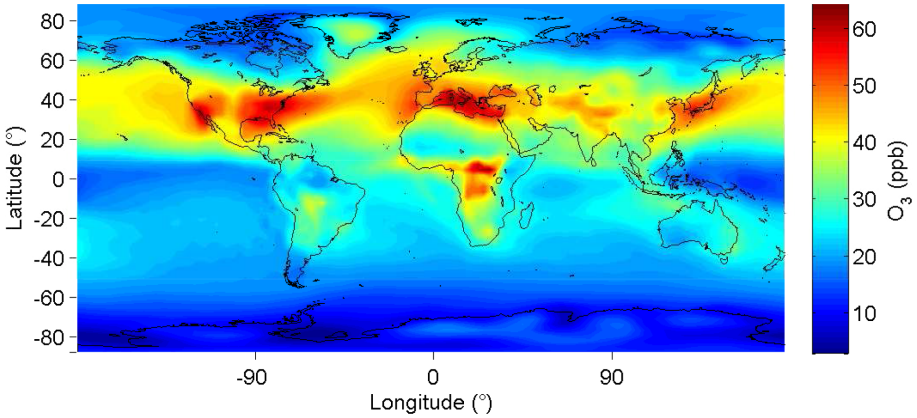

Figure 4. As for Fig. 3a, but for the surface instead of 500 hPa.

ACPD
15, 481–519, 2015

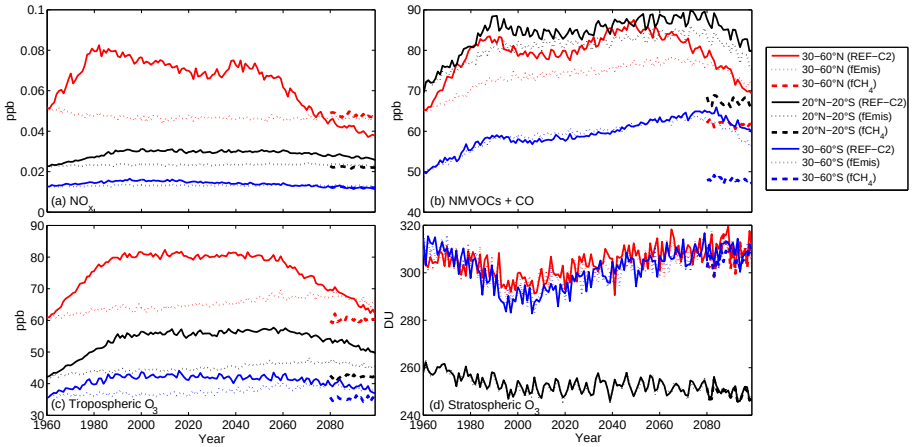

Figure 5. Timeseries of northern midlatitude (30–60° N, red lines), tropical (20° N–20° S, black lines) and southern midlatitude (30–60° S, blue lines): **(a)** NO_x (500 hPa); **(b)** NMVOCs + CO (500 hPa); **(c)** tropospheric ozone (500 hPa); **(d)** stratospheric column ozone. Solid lines: for the REF-C2 simulation. Dotted lines: *f*Emis simulation. Thick dashed lines (2080–2100): *f*CH_4 simulation.

ACPD
15, 481–519, 2015

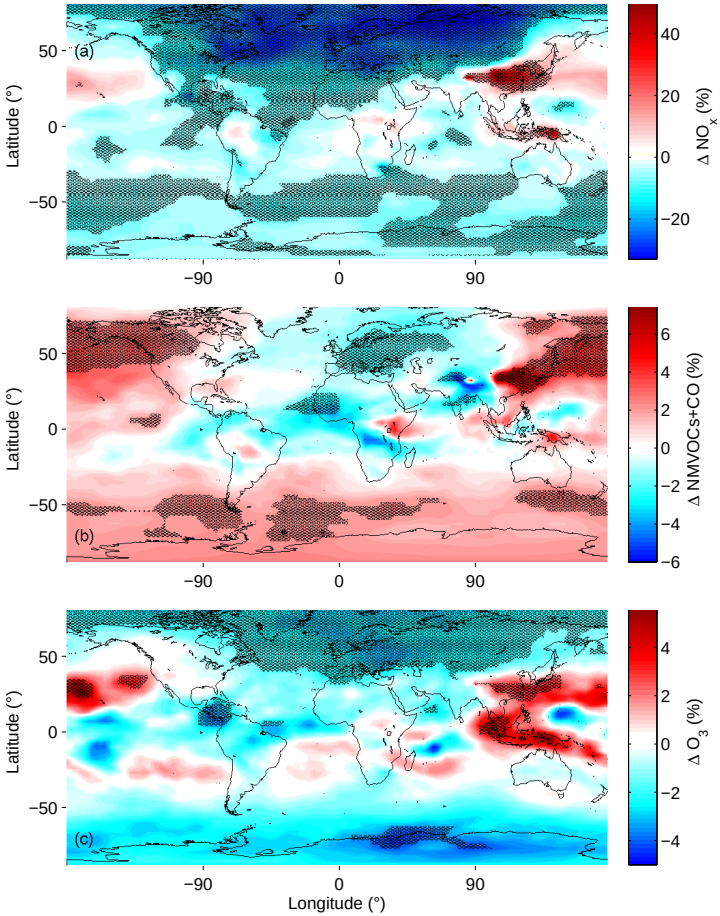

Figure 6. Changes between the 2000s and 2020s decades (2020s minus 2000s) in the REF-C2 simulation at 500 hPa for: **(a)** NO_x; **(b)** NMVOCs + CO; **(c)** ozone. Shading indicates that the difference is statistically significant at the 95 % level of confidence.

ACPD
15, 481–519, 2015

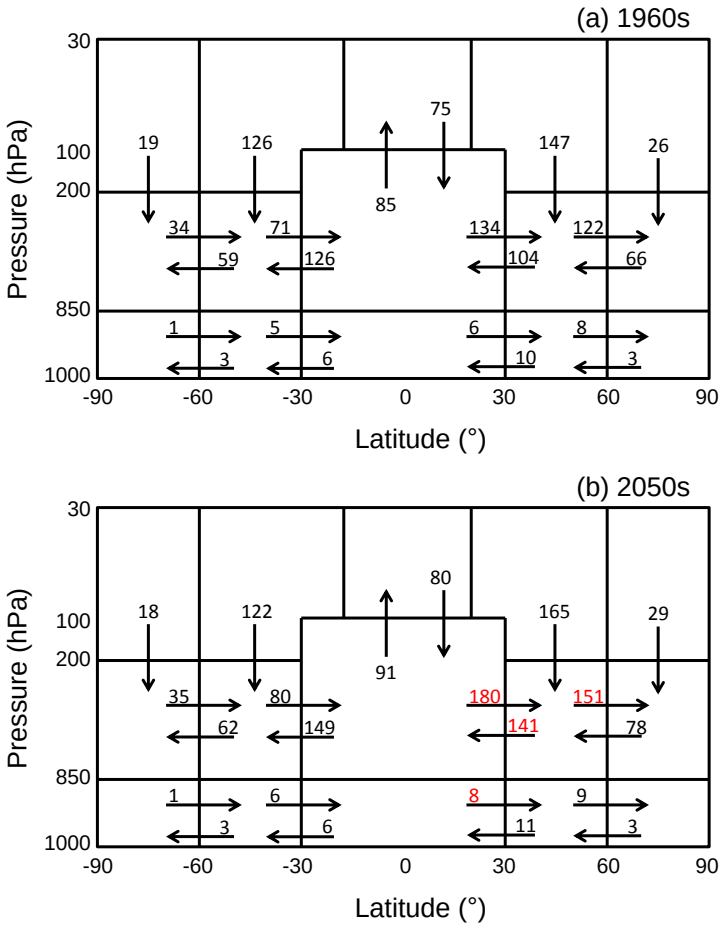

Figure 7. Decadal-mean ozone fluxes (Tg year^{-1}) between defined tracer regions for **(a)** the 1960s and **(b)** the 2050s in the REF-C2 simulation. Red text in panel **(b)** indicates an increase of more than 20 % from the same quantity in **(a)**.

ACPD
15, 481–519, 2015

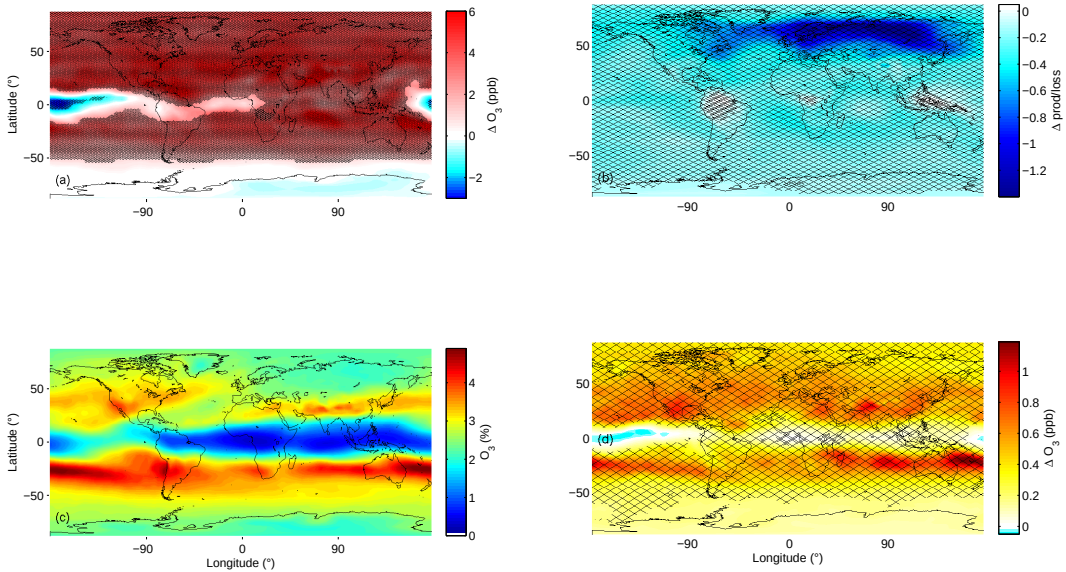

Figure 8. (a) Change in ozone at 500 hPa in the *f*Emis simulation, 2090s minus 1960s; **(b)** change in the ratio of ozone production over loss in the *f*Emis simulation, 2090s minus 1960s; **(c)** percentage of ozone at 500 hPa which was produced in the lower stratosphere in the *f*Emis simulation, 1960s decade; **(d)** absolute change in the amount of ozone at 500 hPa which was produced in the lower stratosphere in the *f*Emis simulation, 2090s minus 1960s. Shading indicates that the difference is statistically significant at the 95 % level of confidence.

ACPD
15, 481–519, 2015

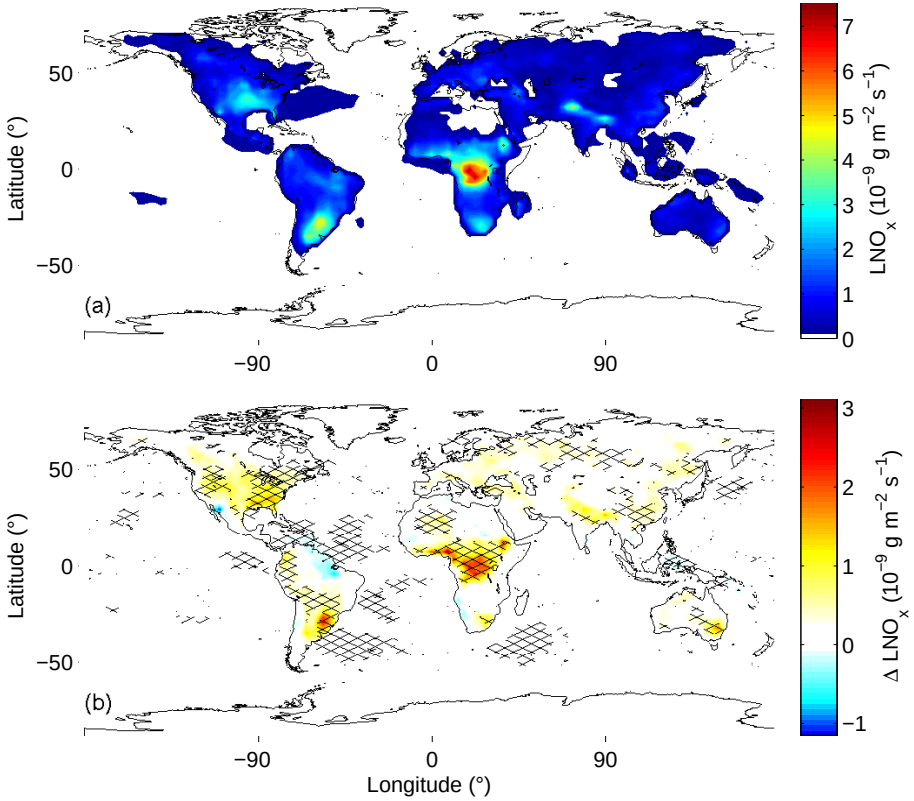

Figure 9. (a) Lightning NO_x emissions in the *f*Emis simulation, averaged over the 1960s; **(b)** change in lightning NO_x emissions in the *f*Emis simulation, 2090s minus 1960s. Shading indicates that the difference is statistically significant at the 95 % level of confidence.

ACPD
15, 481–519, 2015